

Supporting information

Role of Zinc Oxide in the Compounding Formulation on the Growth of Non-stoichiometric Copper Sulfide Nanostructures at Brass-Rubber Interface

Kannan Murugesan Paulthangam,^{†‡} Anirban Som,[‡] Tripti Ahuja[‡] Pillalamarri Srikrishnarka[‡]

Appukuttan Sreekumaran Nair,^{†} Thalappil Pradeep^{*‡}*

[‡]DST Unit of Nanoscience (DST UNS) and Thematic Unit of Excellence (TUE), Department of Chemistry, Indian Institute of Technology Madras, Chennai 600036, India.

[†]MRF Limited, R&D Centre, Tiruvottiyur, Chennai 600019, India.

*For correspondence, E-mail: sreekumaran.nair@mrfmail.com, pradeep@iitm.ac.in

Table of contents

Figures	Title	Page no.
Figure S1	Schematic of laser cut mesh from brass foil	S-2
Figure S2	Large area SEM images and EDS data of vulcanized cords	S-2
Figure S3	AFM of BCSC showing surface roughness	S-3
Figure S4	Graphical representation showing the brass-rubber interface thickness, unaged and aged pull out force	S-3
Figure S5	Physical properties of rubber compound with different ZnO concentrations	S-4

Figure S6	XRD pattern of un-vulcanized brass-coated steel cord	S-5
Figure S7	LED white light image of unreacted and reacted BCSC	S-5
Figure S8	Wagner plots of Cu _{2p_{3/2}} and Zn _{2p_{3/2}} regions at brass-rubber interface for compound identification	S-6
Figure S9	Schematic showing ply region of a radial tire and an enlarged image of the ply region showing the nanostructures interlocking with the rubber compound.	S-7
Table S1	Relative atomic % obtained from XPS	S-7
Table S2	Total crosslink density of rubber compound at different ZnO concentrations	S-8

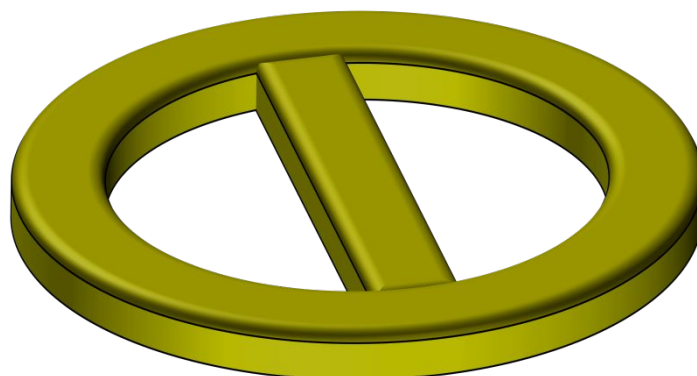


Figure S1. Schematic image of a laser cut mesh from brass foil that was used for interfacial thickness measurement.

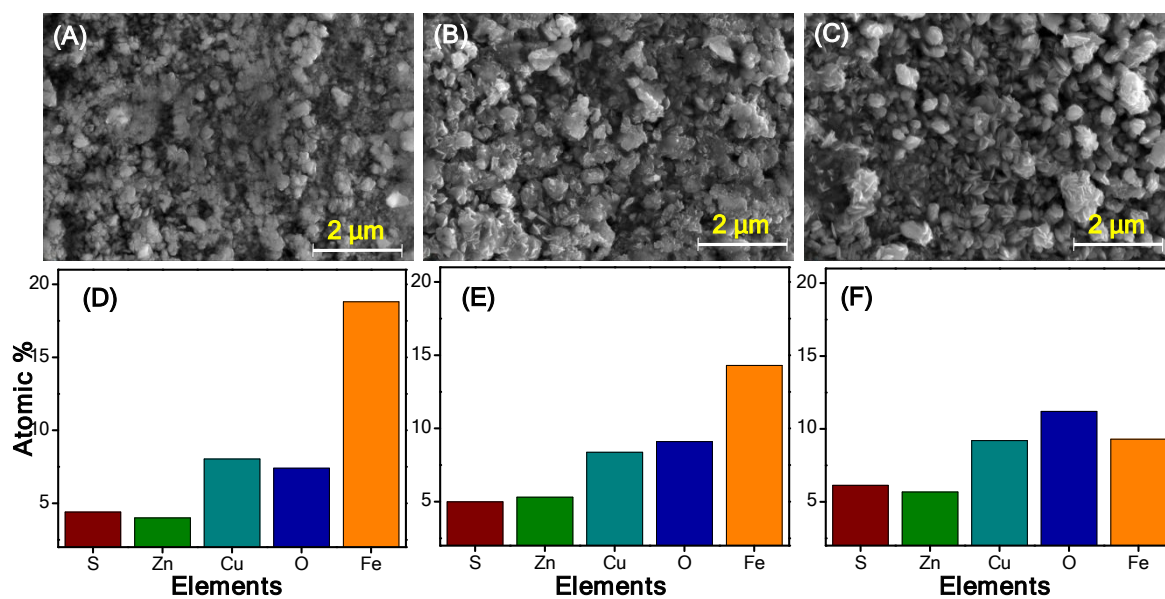


Figure S2. Large area SEM images at (A) 6, (B) 9, (C) 12 PHR ZnO and their corresponding EDX spectra at (D) 6, (E) 9, (F) 12 PHR ZnO.

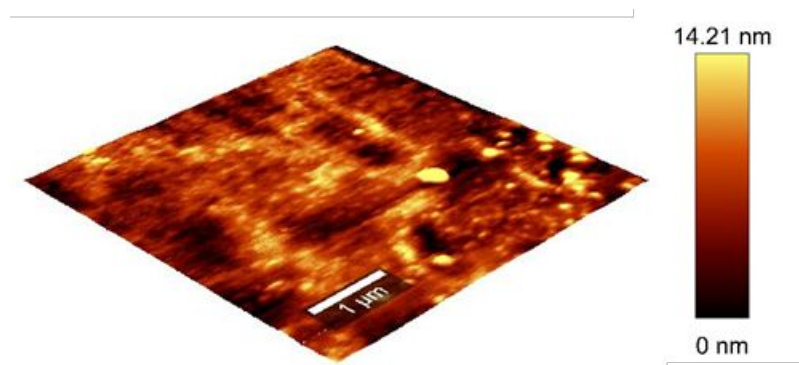


Figure S3. AFM of bare BCSC showing the surface roughness.

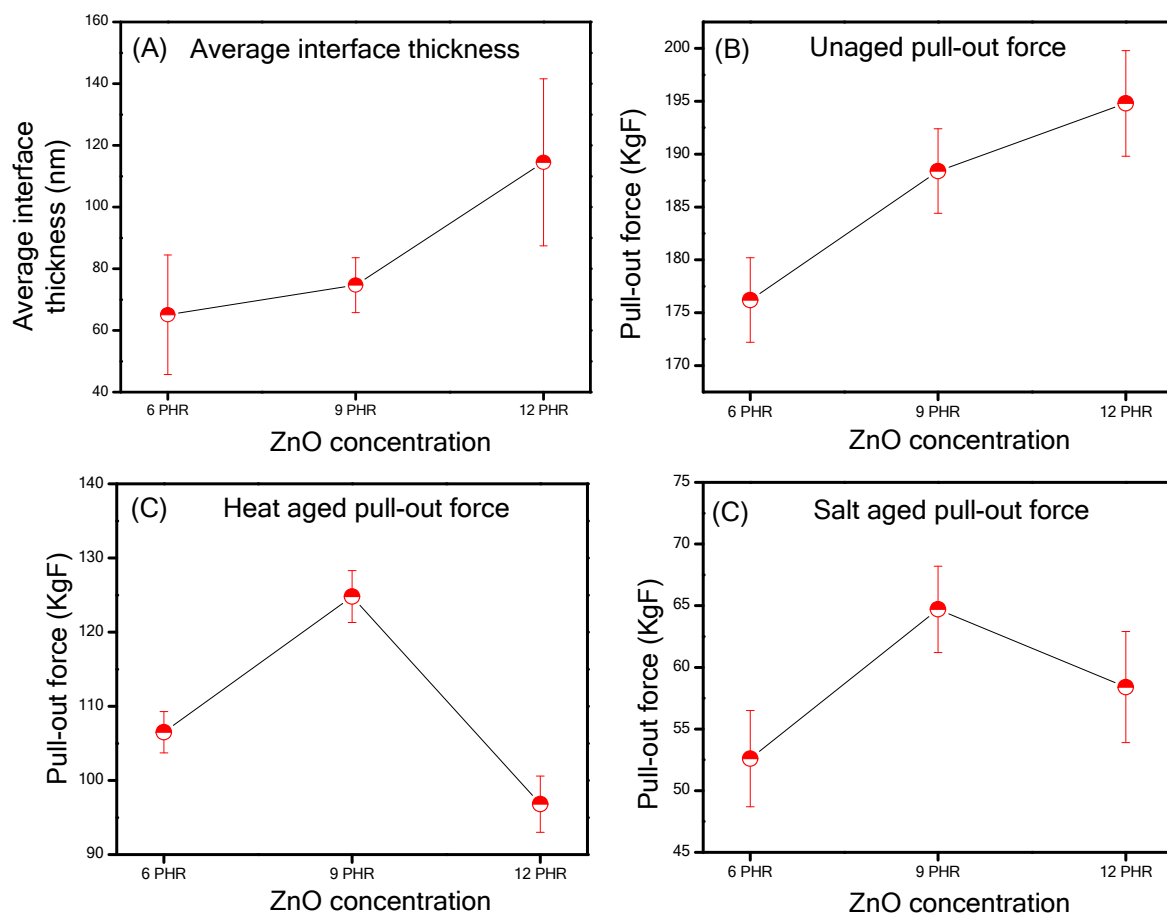


Figure S4. Graphical representation (A) showing the brass-rubber interface thickness with different ZnO concentrations, (B) un-aged, (C) salt-aged and (D) heat-aged pull-out force as a function of ZnO concentrations.

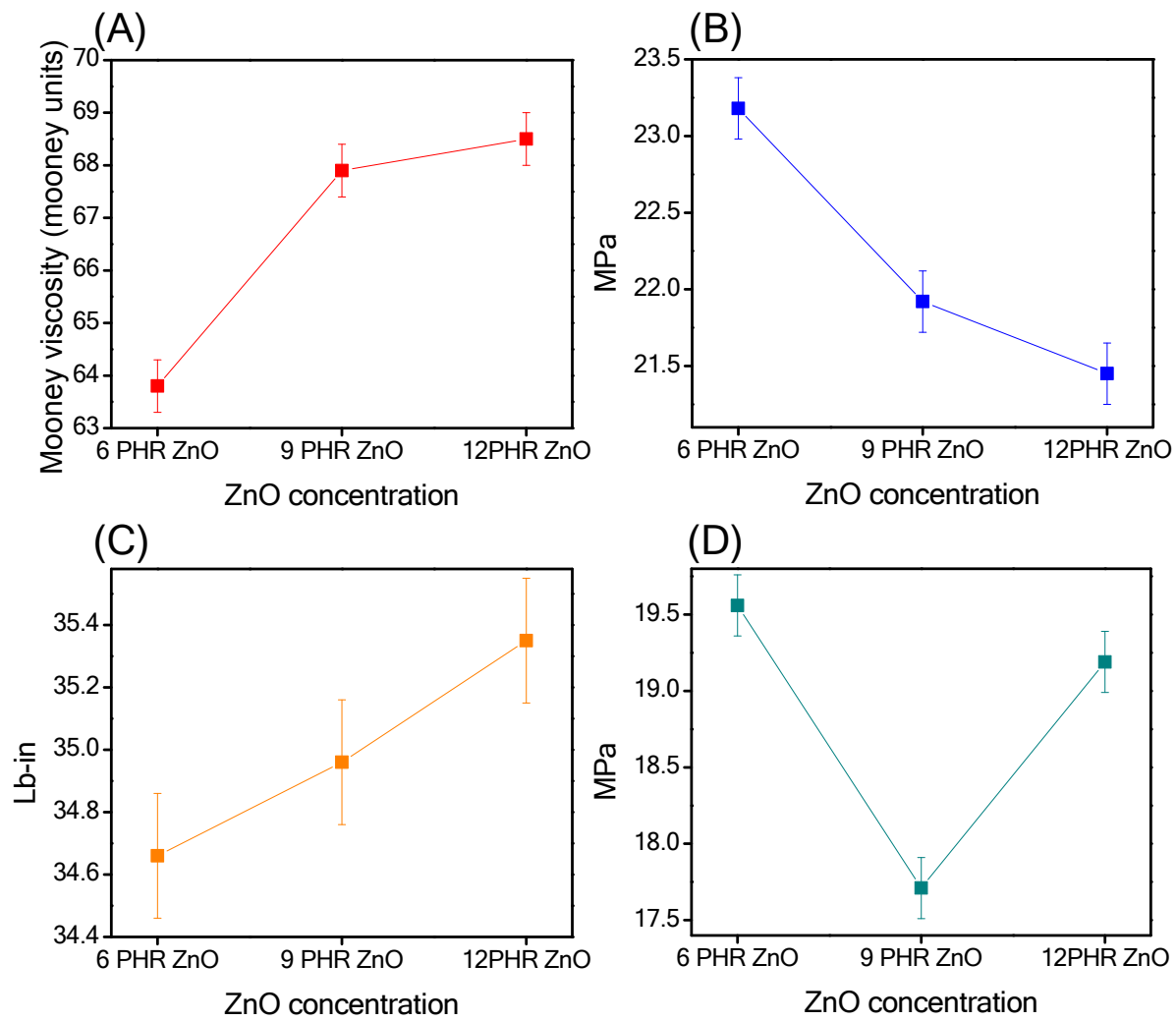


Figure S5. Physical properties of rubber compound with increasing ZnO concentration: (A) Mooney viscosity, (B) tensile strength, (C) moment highest (MH) and (D) 300 % modulus.

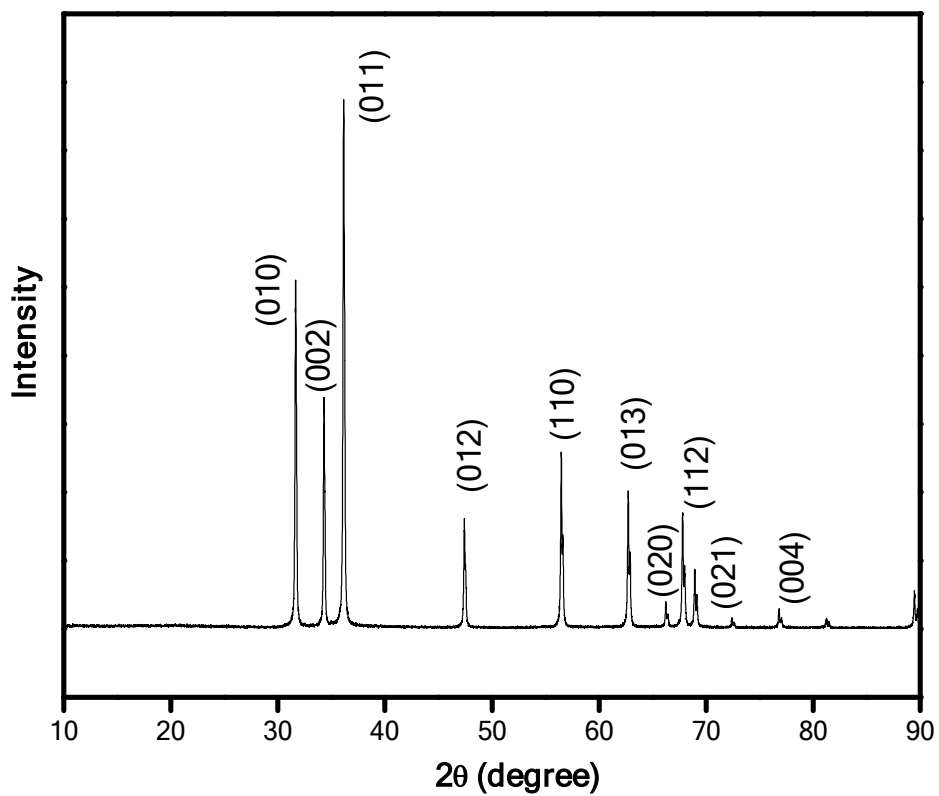


Figure S6. XRD pattern of the ZnO added to the rubber compound.

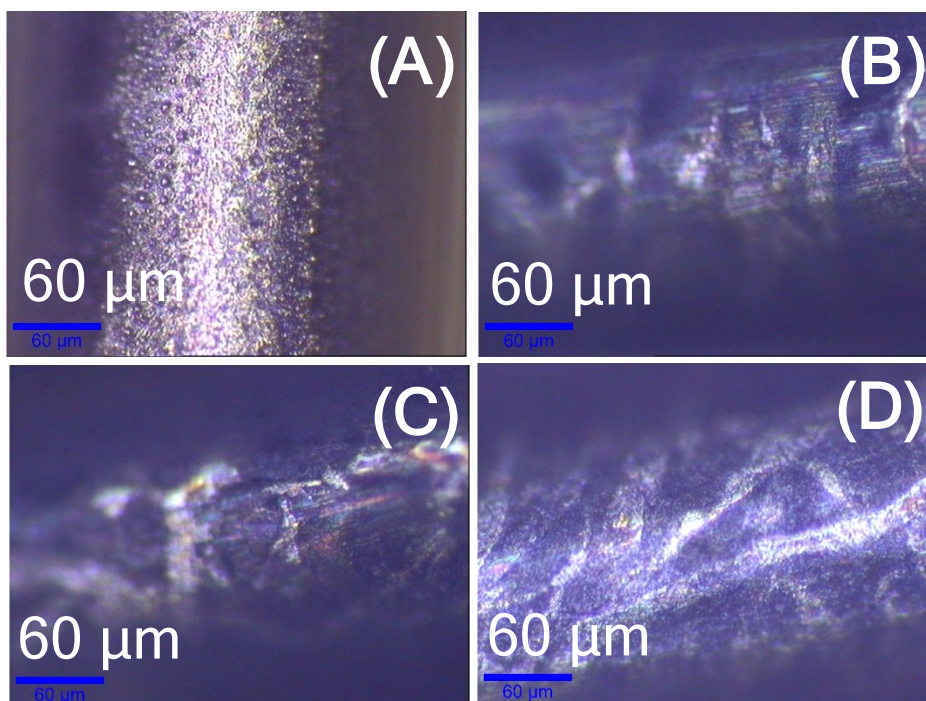


Figure S7. LED white light image of (A) unreacted (B), (C) and (D) vulcanized BCSC with 6, 9 and 12 PHR ZnO.

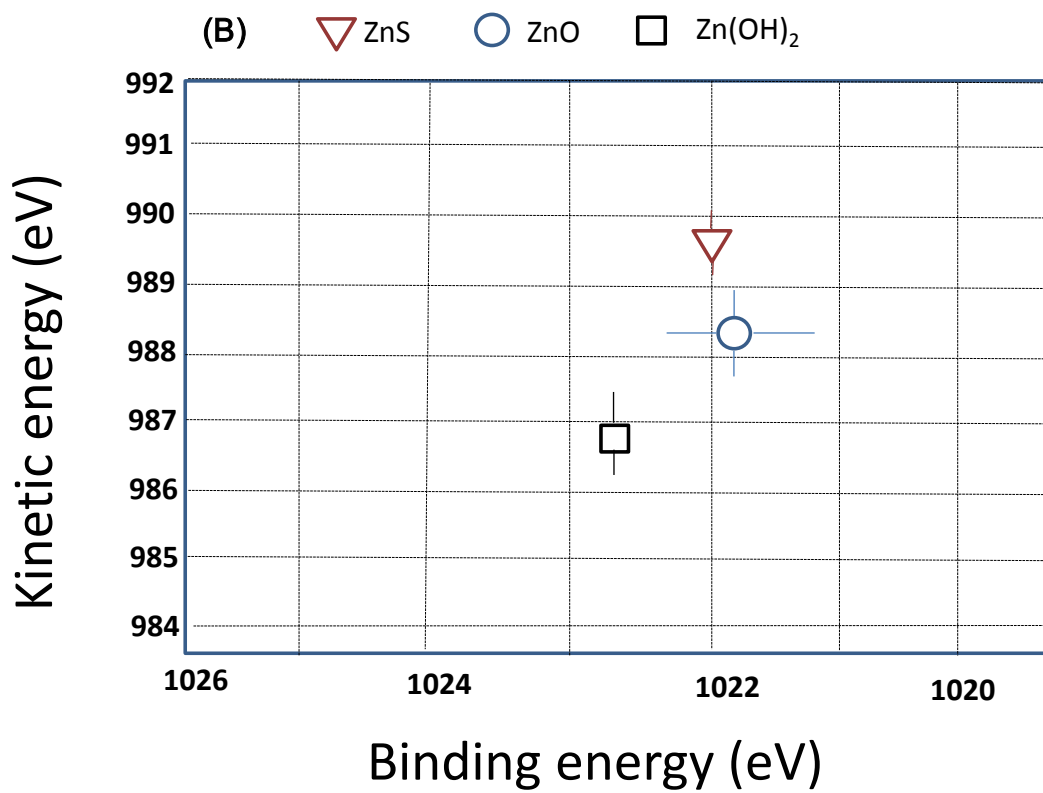
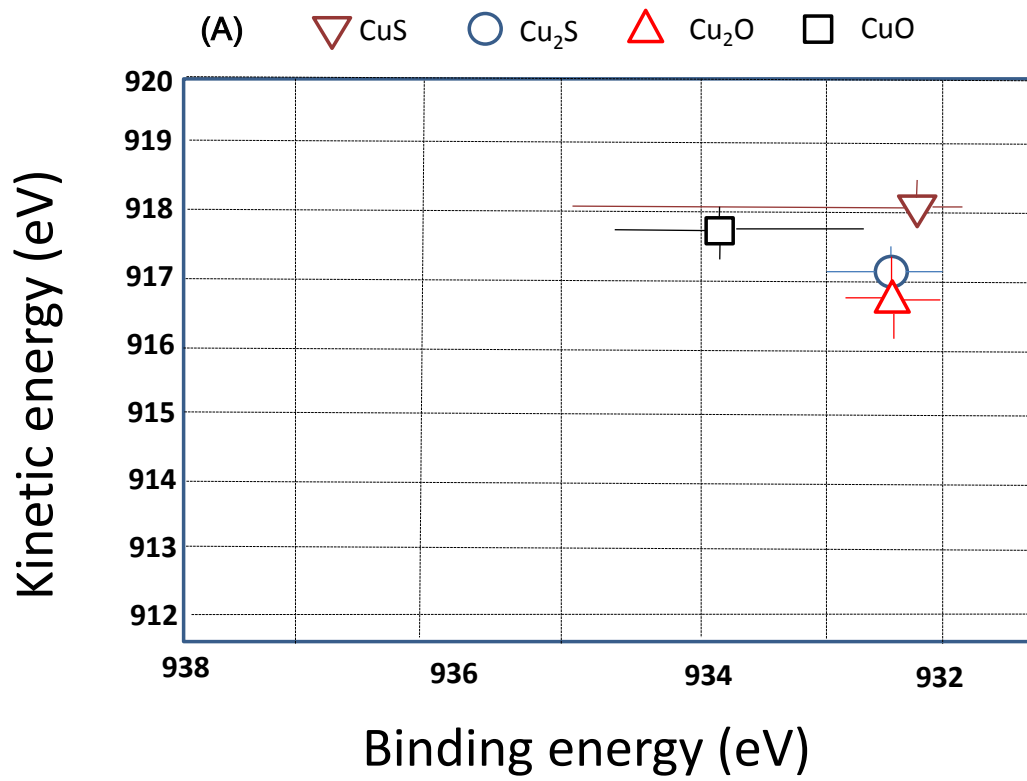


Figure S8. Wagner plots of (A) $\text{Cu}2p_{3/2}$ and (B) $\text{Zn}2p_{3/2}$ regions for compound identification at brass-rubber interface. Adapted from references 35 and 36 in the main text.

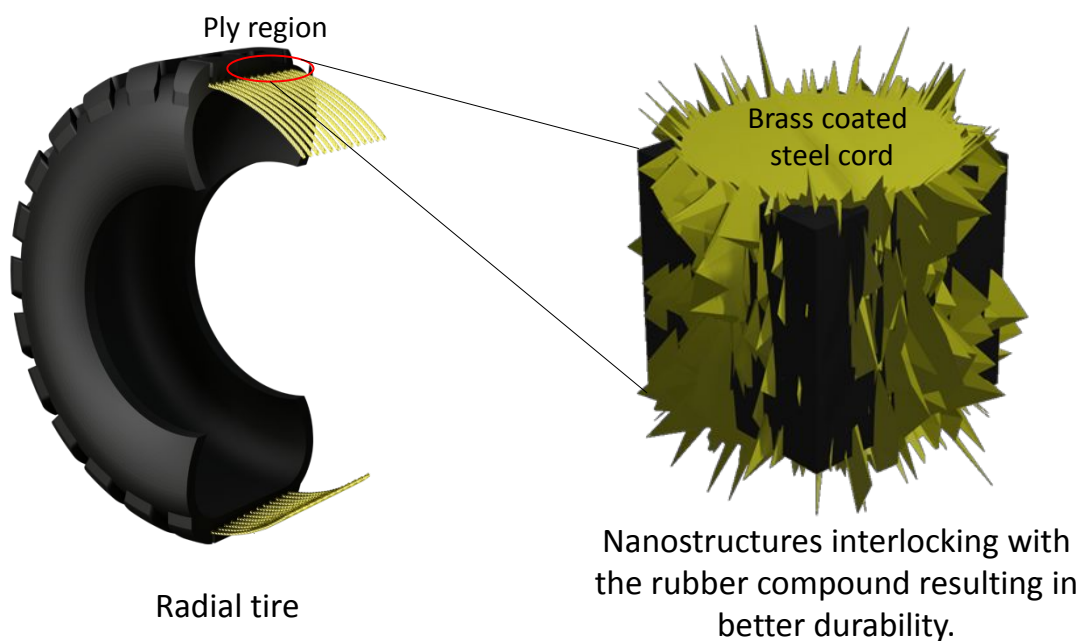


Figure S9. Schematic showing ply region of a radial tire and an enlarged image of the ply region showing the nanostructures interlocking with the rubber compound.

Table S1. Total crosslink density of rubber compound at different ZnO concentration.

ZnO concentration (PHR)	Total crosslink density (mol/cc)
6	2.61 E-5
9	3.09 E-5

12	3.44 E-5
----	----------

Table S2. Relative atomic % obtained from XPS.

Element	6PHR ZnO	9PHR ZnO	12PHR ZnO
Cu	1.43	1.46	1.77
Zn	1.92	2.15	2.93
S	1.64	1.68	1.87
O	9.27	12.25	13.33